JOURNAL OF GEOPHYSICAL RESEARCH, VOL. 106, NO. A8, PAGES 15,445–15,454, AUGUST 1, 2001

Relation between optical emissions, particles, electric fields, and Alfvén waves in a multiple rayed arc

Thomas J. Hallinan,[1] J. Kimball,[2] H. C. Stenbaek-Nielsen,[1] K. Lynch,[3] R. Arnoldy,[3] J. Bonnell,[4] and P. Kintner[5]

Abstract. Velocities of rays in auroral arcs were used to infer the perpendicular electric fields above the acceleration region. Using rocket measurements of electron energy as a proxy for the high-altitude potential, the high-altitude perpendicular electric fields were calculated and found to be in good agreement with those derived from the ray motions. Additionally, a 0.6 Hz oscillating electric field at high altitude was postulated on the basis of the passing rays. Such a field was also calculated from the electron energy measurements and was found to be closely related to an Alfvén wave measured on the payload following a delay of 0.8 s. The measured electron energy flux agreed well with the auroral luminosity down to scale sizes of about 10 km. The combination of ground-based imaging and the measured energy flux also allowed a determination of the lower border altitude of the arcs. They were found to be somewhat higher (130 km) than expected on the basis of the electron energy. A tall rayed arc with a lower border height of 170 km was associated with a burst of suprathermal electrons on the poleward edge of the aurora.

1. Introduction

Inverted V electron spectra in auroral arcs are usually interpreted as signatures of V-shaped equipotential contours on the field lines above the arc. This potential distribution is assumed to accelerate the electrons downward toward the atmosphere, thereby providing the peaked energy distribution. An additional characteristic of such a potential distribution is the existence above the acceleration region of a strong convergent perpendicular electric field. The convergent electric field has also been inferred from the Kelvin-Helmholtz vortices (auroral rays) in arcs [*Hallinan and Davis*, 1970] and from the countervailing drift motions of the auroral rays in adjacent arc elements [*Hallinan and Davis*, 1970; *Carlqvist and Bostrom*, 1970]. The convergent field is often measured by satellites operating above the acceleration region (above 1-2 R_E) [*Mozer et al.*, 1977].

There is good qualitative agreement between the convergent electric field measured by high-altitude satellites, the field inferred from electron spectra measured by rockets or low-altitude satellites, and the field inferred from ground-based observations of auroral vorticity and ray motions [*Swift et al.*, 1976]. Nonetheless, it has proven extraordinarily difficult to check for quantitative agreement within an individual auroral arc. The difficulty is that the three types of measurements occur in vastly different regions of space. The electric field measurements must be made above the acceleration region, typically above about 10,000 km altitude. The electron spectra must be measured below the acceleration region, typically below about 6000 km altitude. The visual aurora (although responding to electric fields above the acceleration region) occurs in the lower ionosphere and the high-resolution imaging necessary to observe the ray formation and motions is presently done only from the ground or from aircraft. For proper observation the rays must be within about 30 km of the local magnetic zenith at the camera location.

The AMICIST rocket flight from Poker Flat, Alaska, provided a rare opportunity to make quantitative comparisons between electric fields inferred from the electron spectra and those inferred from auroral ray motions. In addition, the modeled electric field in the acceleration region above the drifting auroral rays appears to be the source of Alfvén waves measured at the payload at an altitude of 860 km. Finally, the in situ data were combined with the image data to determine the altitude of the lower border of the aurora and to compare that with the altitude predicted from the measured energy spectrum.

2. Experiment

2.1. Instrumentation

The AMICIST payload was launched from Poker Flat Research Range on February 24, 1995. It flew over a multiple rayed arc that was overhead at Kaktovik on the north coast of Alaska. Optical instrumentation at Kaktovik included an intensified CCD all-sky television camera, and an intensified CCD narrow-field TV camera, both operating in white light. The narrow-field camera was aimed at the 110 km footprint of the payload trajectory, utilizing a real-time trajectory prediction program. Both cameras were recorded on 3/4 inch videotape at the National Television Systems Committee (NTSC) rate of 30 frames per second, and both included time, synchronized to the time standard used by the Poker Flat telemetry station.

[1]Geophysical Institute, University of Alaska, Fairbanks, Alaska.
[2]Johnson Space Center, Houston, Texas.
[3]Space Science Center, University of New Hampshire, Durham, New Hampshire.
[4]Space Science Laboratory, University of California, Berkeley, California.
[5]School of Electrical Engineering, Cornell University, Ithaca, New York.

Paper number 2000JA000321.
0148-0227/01/2000JA000321$09.00

Figure 1. All-sky image of arcs during overhead passage of Amicist payload. The most poleward of the three arcs (c) is close to the magnetic zenith at Kaktovik.

The payload instrumentation is described more fully by *Lynch et al.* [1996] and *Bonnell et al.* [1996]. The payload was in two sections, separated near apogee (over Kaktovik) by about 300 m. Both sections included ion and electron detectors, magnetometers, and wave measuring systems. The main payload also included 5.5 m Weitzmann booms with 1.3 m flip-down extensions for measuring low-frequency and DC electric fields.

2.2. Video Analysis

Angular calibrations for the auroral images were determined by matching the observed stars to the Smithsonian Astrophysical Observatory catalog. For purposes of comparison between the payload data and the video images, all rocket positions were traced along the geomagnetic field to the lower ionosphere. As will be shown later, the best fit was obtained by assuming a lower border altitude for the aurora of 130 km. However, the choice of a reference altitude is not critical to the discussion of auroral motions as long as the same altitude is used for calculating both auroral motions and the motion of the footprint of the rocket payload. Positions, dimensions, and velocities of auroral forms were calculated from the angular positions assuming an altitude of 110 km.

2.3. General Auroral Situation and Rocket Trajectory

The payload was launched into a large-scale active omega-shaped band and, near apogee, intersected a series of three discrete arcs (labeled from south to north as A, B, and C in Figure 1). The arcs had faded to about 10 kR in the green line by the time of the encounter. Smaller-scale structures within the arcs such as rays and folds had a generally indistinct quality. Arc C was aligned at an angle of 57° to the trajectory. The equatorward and poleward arcs (A and C) had large-scale folds as well as smaller-scale features. These small features were visible as rays in arc A. In arc C, which was closer to the magnetic zenith, they were recognizable as counterclockwise Kelvin-Helmholtz vortices (curls) as described by *Hallinan and Davis* [1970]. The rays in arc A were presumably also curls but were too far from the magnetic zenith to observe their internal structure. They drifted westward, while the curls in arc C drifted eastward. Arc B showed a hint of internal striations parallel to the arc but was otherwise unstructured. The arcs and their internal features are shown schematically in Figure 2.

The poleward arc (C) was very close to the local magnetic zenith at Kaktovik. Specifically, the portion of the arc within the field of view of the narrow-field camera came within 13 km of the magnetic zenith, and the 110 km footprint of the payload intersected the arc approximately 30 km to the west of the magnetic zenith, at the edge of the field of view of the narrow-field camera. At the time of the encounter the rocket was at an altitude of about 860 km. The velocity of the 110 km footprint of the payload was 1.2 km s^{-1} and the component perpendicular to the arcs was 1.0 km s^{-1}.

Just after the payload passed through the aurora, there were

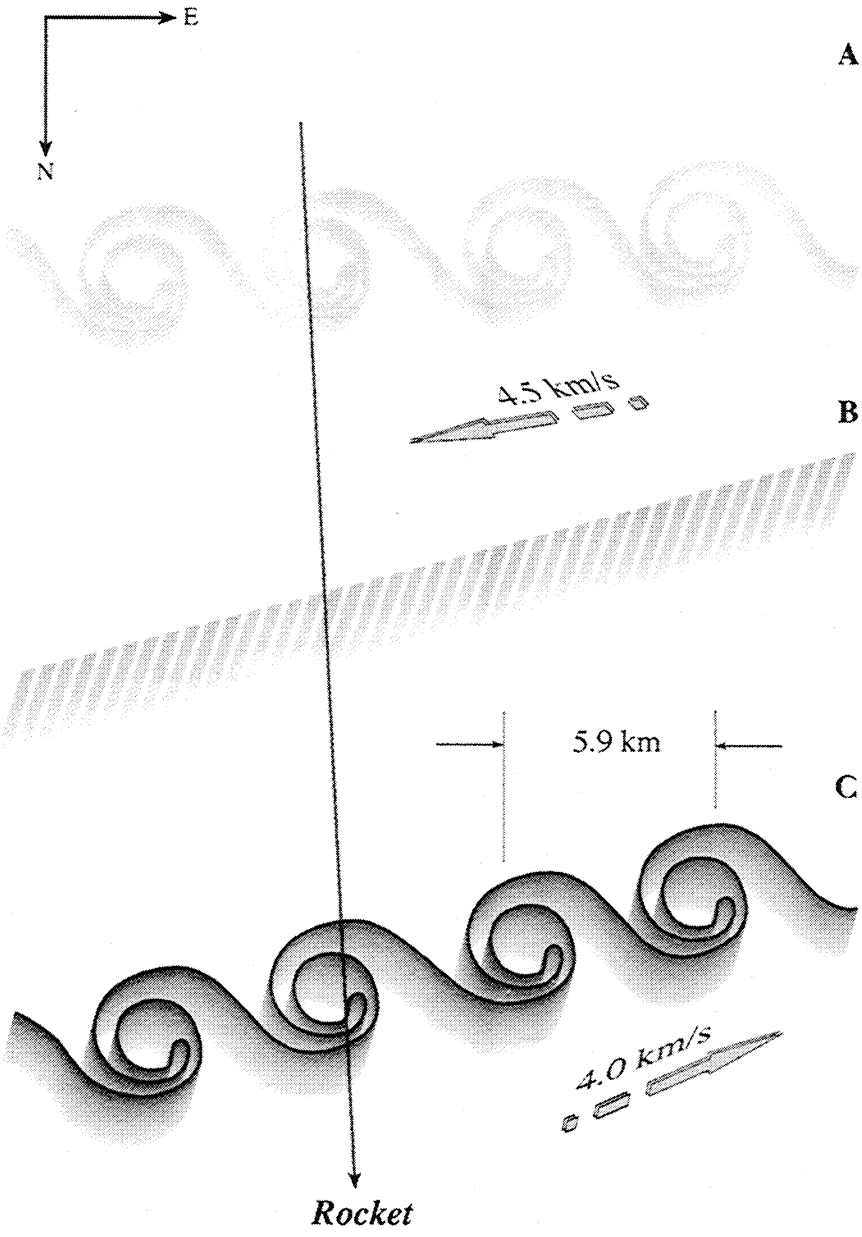

Figure 2. Schematic of Amicist multiple arc.

two brief activations including brightening and ray motions along the poleward arc (+431 s and +443 s). The first of these was associated with a transient tall rayed arc that formed poleward of the previous aurora and was intercepted by the payload.

2.4. Auroral Motions and Microstructure

The listed times give the time after launch in seconds and correspond to passage of the payload through the described features or to the time of particular auroral events. Figure 2 summarizes the observations of the multiple arc in schematic form.

2.4.1. Time after launch, 359-375 s. The equatorward arc (A) had several medium-scale folds drifting westward. The payload passed through a bright spot corresponding to the eastern end of a fold. The arc was at 60° elevation angle and appeared in the narrow-field camera as a basically homogeneous arc with some vague field-aligned rays, also drifting westward. The ray velocity was measured as 4.5 ± 1 km s^{-1}. The large error bar reflects the ill-defined nature of the rays. There is also a hint that the arc may be further subdivided into two arc elements, but it is too far out of the magnetic zenith to be sure.

2.4.2. Time after launch, 390-405 s. The central arc (B) is weaker and does not exhibit internal motions. The arc does, however, contain low-contrast east-west aligned striations.

2.4.3. Time after launch, 411-420 s. The poleward arc (C) was the most active of the three. At the time of conjunction there was a bright fold drifting eastward along the arc and simultaneously brightening. It appears to have reached the rocket trajectory just in time to intercept the payload. The nominal location of the payload footprint was just at the western edge of the narrow-field camera field of view. The exact location of the payload footprint is uncertain because of east/west uncertainty (±6 km) in the mapping along the geomagnetic field in the presence of possible auroral Birkeland currents. Simultaneously

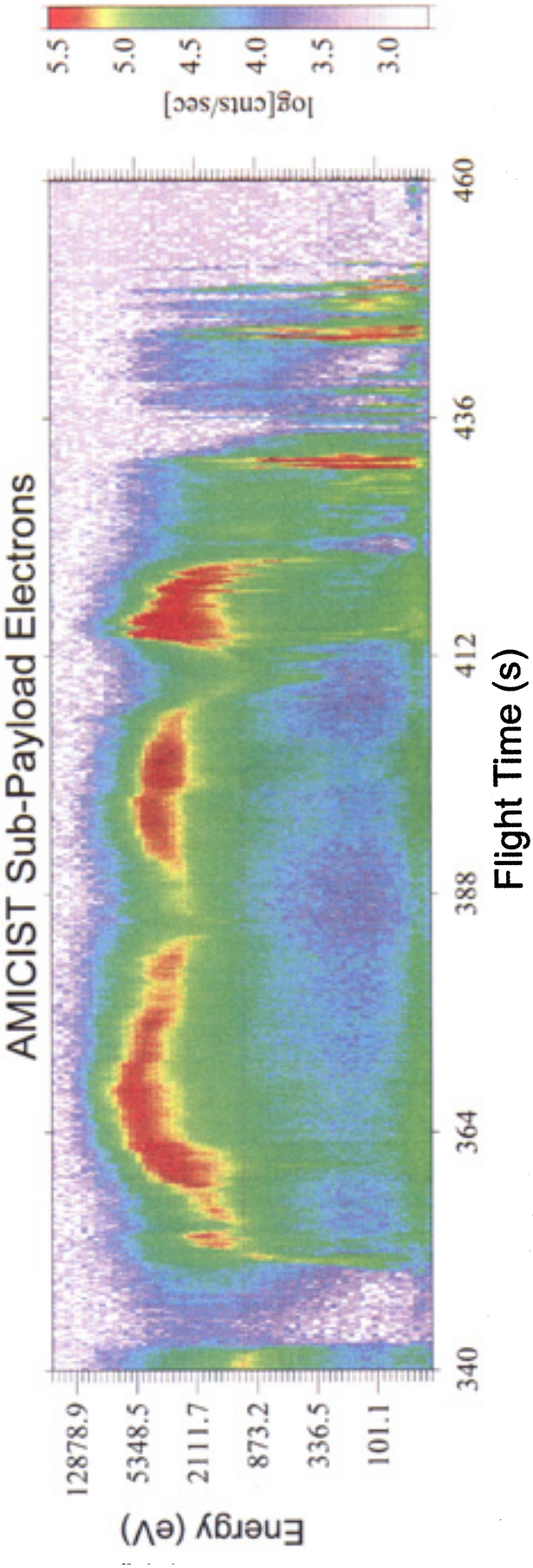

Plate 1. Electron Energy Spectrum for AMICIST. The three arcs are seen as structure within a broad inverted V.

with the intercept a Kelvin-Helmholtz vortex array drifted eastward through the payload footprint. Because the vortex street was not in the magnetic zenith, the vortices were not as well defined, as is often the case, but were still easily identifiable. The individual vortices were counterclockwise in shape, as is always the case in the Northern Hemisphere [*Hallinan and Davis*, 1970]. The spacing between the vortex centers was 5.9± 0.7 km and the vortices (curls) were drifting eastward at 4.0 km s^{-1}, giving a frequency of 0.68±0.08 Hz. (It should be noted that, since the payload footprint was at the edge of the field of view, these measurements were made at a point 5-10 km to the east of the payload.)

2.4.4. Time after launch, 430-450 s. At 431 s and at 443 s there were brief (~3 s) activations of rays in and just poleward of arc C. The most poleward rays were tall, indicative of low-energy precipitation. At 431 s the payload was apparently in the tall rays and about 10 km poleward of more actively moving Kelvin-Helmholtz vortices. At 443 s the payload was poleward of the visible aurora.

2.5. Electron Data and Arc Intensities

Plate 1 shows the electron spectrogram from the main payload covering the period from 340 to 460 s. The three arcs discussed above show as a small modulation in the inverted V between 350 and 430 s. The transient events at 431 and 443 s are characterized by lower energy electrons which are spread in energy.

As shown by *Stenbaek-Nielsen et al.* [1998], a linear plot of total electron energy flux (shown in Figure 3 for the period 340-440 s) is more useful for comparison with the optical data. Here the three separate arcs are readily visible. Superimposed on the energy flux plot is a plot of the relative optical intensity measured along the moving footprint of the rocket trajectory. With single-station data, it is impossible to completely determine the altitude and location of the aurora. If one assumes an altitude for the auroral emission, then the location is determined. Since this altitude was unknown, our procedure was to try assuming different altitudes until we found the best match between the optical intensity distribution and the energy flux measured at the rocket. Arc C is close to the magnetic zenith, so its position in the optical plot is relatively insensitive to the choice of altitude for the footprint. On the other hand, the position of arc A in the plot is sensitive. Best agreement was found by choosing an altitude of 130 km. As seen in the plot, the transient event at 431s is not matched with this assumed altitude. It was found that this event matched by assuming an altitude of 170 ± 10 km for the lower border. A more detailed modeling planned for the future will include the expected distribution in altitudes from the measured electron energies.

The effective resolution of the plot from the all-sky TV camera, expressed in terms of plus count, is the width of a pixel in kilometers divided by the component of payload footprint velocity perpendicular to the arcs and is about 1.4 s. The structured electron flux within arc C is connected with the moving rays that are not resolved in the all-sky data but are seen in the narrow-field images (not shown). The structure in arc B is not apparent in the all-sky image but is seen in the narrow-field data as two east-west striations within the arc.

2.6. Electric and Magnetic Field Data

Roughly corresponding to the passage of the payload through arc C (410-420 s), a wave was detected at the payload in both the electric and magnetic components as shown in Figure 4. Figure

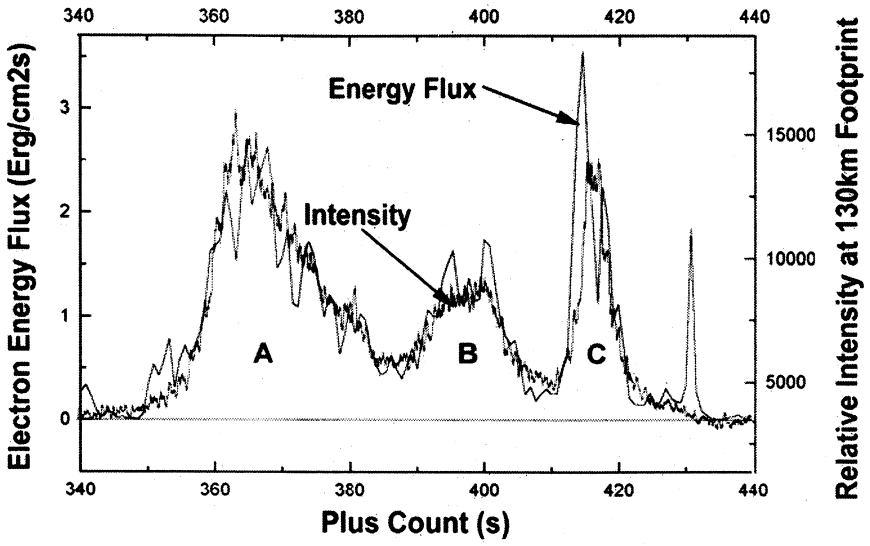

Figure 3. Electron energy flux measured on the main payload as it traverses arcs A, B, and C in Figure 1. Superimposed on the plot is a plot of the relative intensity of the arcs as measured in the all-sky TV camera following the 130 km footprint of the payload.

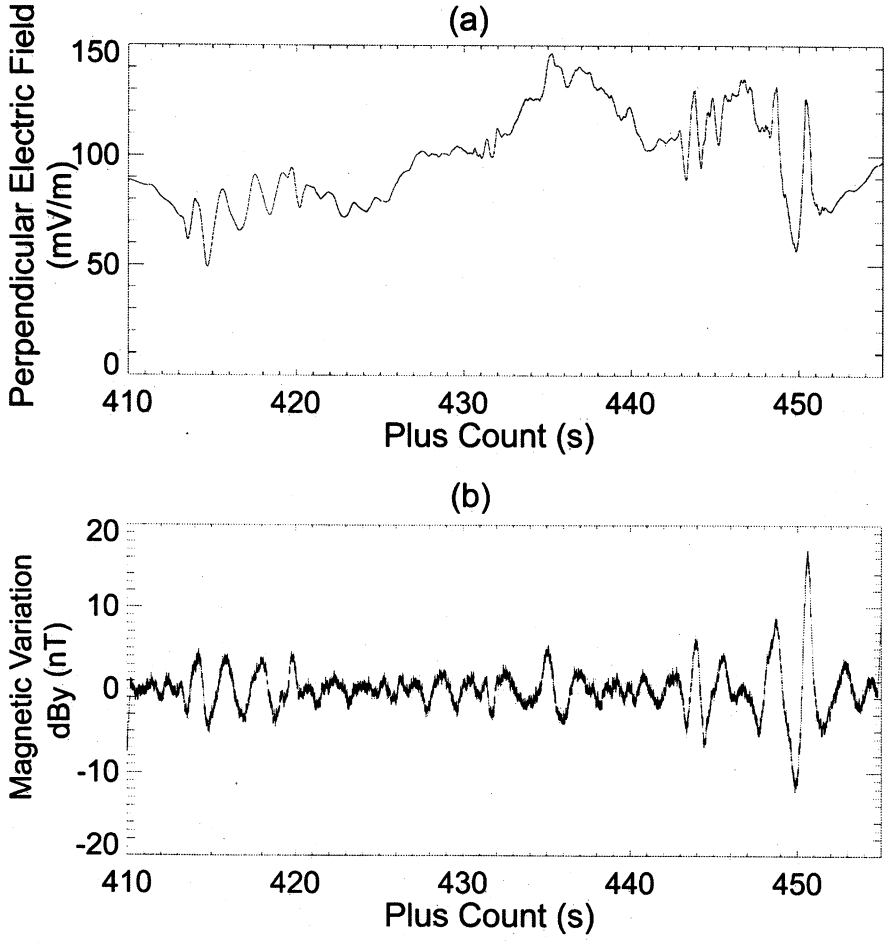

Figure 4. Perpendicular Electric field (Positive westward) and magnetic perturbations (Positive northward) measured on the main payload.

4a shows the variation in the component of the electric field perpendicular to both the geomagnetic field and the payload trajectory. A positive value points approximately magnetic west. The v x B electric field due to payload motion has not been removed. Figure 4b shows the magnetic perturbations for the same period. A positive value points along the spin axis, approximately magnetic north. The poynting flux E x δB is downward for in-phase signals.

The $\delta E/\delta B$ ratio yields a velocity of 4500 km s^{-1}, somewhat less than the Alfvén velocity (7360 km s^{-1}) calculated using a plasma density derived from the measured lower hybrid frequency and an assumed ion composition of 90% O^+ and 10% H^+. Also, δB was observed to lag δE by about 0.2 s. The smaller δE values and the phase lag of δB are at least qualitatively consistent with a model in which an Alfvén wave is partially reflected from the ionosphere below the rocket, and the payload samples a composite of the incident and reflected waves. Similar waves were seen associated with the transient events at 431 and 443 s and were interpreted by *Bonnell* [1997] as being Alfvén waves.

3. Discussion

3.1. Energy Flux and Visible Arcs

The superimposed plots in Figure 3 show excellent agreement between the normalized intensity of the aurora and the electron energy flux, with regard to the locations, widths, and relative intensities of the three arcs. This emphasizes that a linear plot of the electron energy flux is a good indicator of what is seen visually.

The intensity plot was produced by sampling the all-sky video along the moving magnetic footprint of the payload. To do this, it was necessary to have an accurate payload trajectory and to assume the correct altitude for the footprint. Since arc C was so close to the magnetic zenith, the footprint of the payload in this arc was essentially independent of the assumed altitude. Hence we could verify the accuracy of the payload trajectory by noting that arc C matched the location of the energy flux peak. But the matching of peak A was highly sensitive to the assumed altitude, and a good match was obtained only by assuming an altitude of 130 km.

The altitude of peak optical emission is determined by the energy of the electrons. In Figure 3 (and later in the paper in Figure 5c) it can be seen that the energy in arc A is 4-5 keV. According to the models of *Rees* [1963] or of *Banks et al.*[1974] this should produce a peak luminosity at about 115 km with the lower border a bit lower. An altitude of 130 km appears in these models to be more consistent with an energy of about 2 keV. This discrepancy is not understood and will be studied more intensively as a future project.

The tall rays seen at 431 s had a lower border of 170±10 km The high altitude and the length of the rays are at least qualitatively consistent with the measured electron energies spread fairly uniformly from 100 to 800 eV. Again, detailed modeling will be a future project.

3.2. Electric Potential Distribution

For simplicity we will consider the case of a straight and uniform magnetic field. If the energy of the auroral electrons is derived primarily from an electrostatic potential, the plot of peak electron energy versus time (distance along the trajectory) can be regarded as a profile of the potential distribution above the arc.

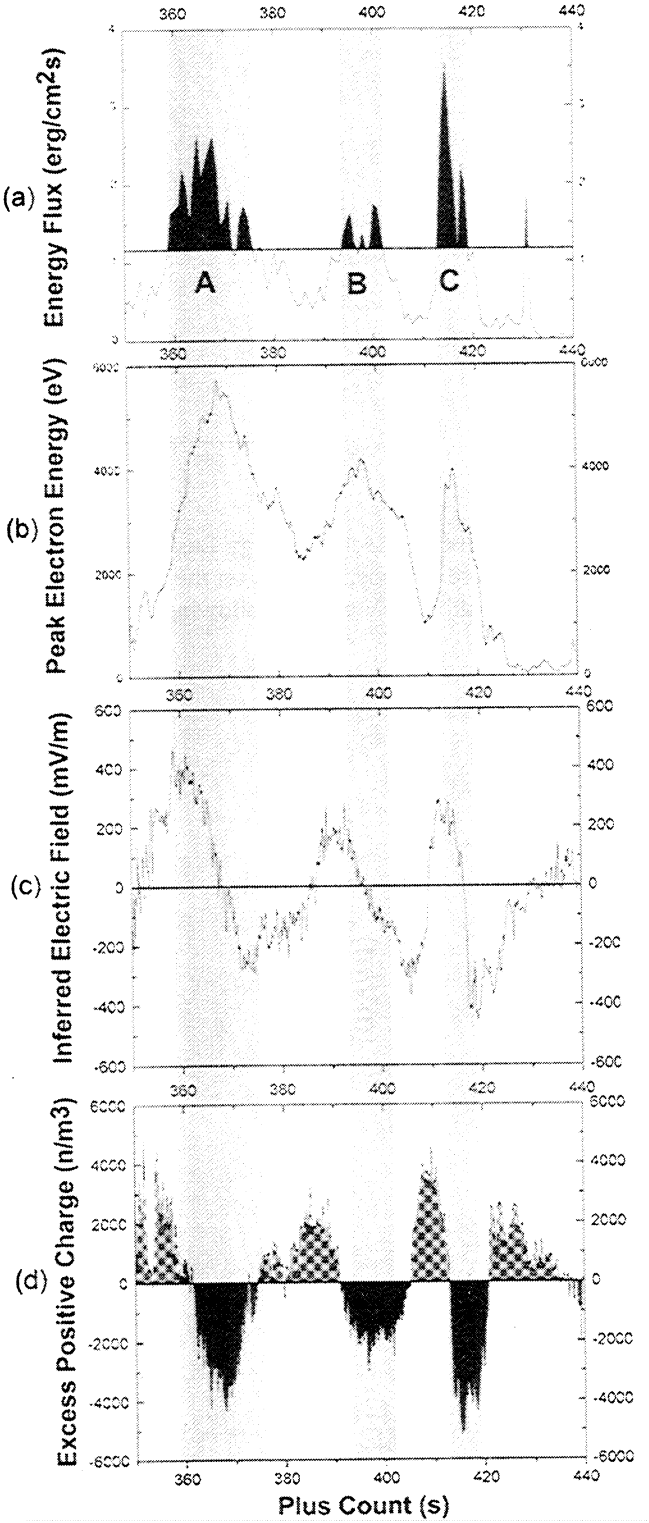

Figure 5. Electron energy flux; energy of "monoenergetic" peak; inferred electric field calculated from the derivative of the energy peak; interred charge density calculated from the 2nd derivative of the energy peak. Shaded regions indicate the visible arcs (energy flux somewhat greater than one erg/cm²s).

Correspondingly, the spatial derivative of the energy plot is a measure of the component of the electric field parallel to the rocket trajectory but along a cut above the acceleration region. Similarly, the second derivative is a measure of the excess charge density above the acceleration region. Despite some internal motions and some changes in intensity, the overall structure was relatively stable during the 90 s required for the complete passage through the arcs. Hence we will for now assume that the measured derivatives from the electron data are spatial rather than temporal. For electron energy we use the energy at which the peak differential energy flux occurs.

Specifically, the inferred perpendicular electric field from the electron energy is given as

$$E_y = (\delta w/\delta t)/(\delta y/\delta t)$$

and the excess charge density is

$$\rho = -\varepsilon_0 (\delta E_y/\delta t)/(\delta y/\delta t)$$

where E_y is the perpendicular electric field, w is the energy of the peak electron flux in electron volts, $\delta y/\delta t$ is the velocity of the payload footprint perpendicular to the arc (1.0 km s^{-1}), and ρ is the charge density in electrons m^{-3}.

Figure 5 shows the potential, electric field, and charge density inferred from the electron energy. For reference the top panel shows again the energy flux. The regions above about 1.3 erg $cm^{-2}s^{-1}$ correspond roughly to the visible arcs and are shaded in the figure. In the second panel the potential is seen to peak within each arc, although not returning to zero between the arcs.

The third panel shows the inferred high-altitude electric field (above the acceleration region). Because the differentiation amplified the noise in the data, it was necessary to do some smoothing. Accordingly, the peak fields have been diminished somewhat and localized fields associated with individual vortex streets have been smoothed over. Nonetheless, the plot retains the main features of the arcs: a negative slope (counterclockwise vorticity in the E x B drift) within each arc and peak fields at the edges of arcs A and B of $\pm$ 400 mV m^{-1}.

The vortices (rays) tend to form in thin filaments near the outer edges of the arcs. Near the edges of arcs A and C there are fields of the order of 400 mV m^{-1} in opposing directions. These should produce maximum velocities of around 8 km s^{-1} westward in the equatorward arc and eastward in the poleward arc. Curls spin in a counterclockwise direction while moving along the arc. Hence their motion is somewhat analogous to that of a bicycle wheel that rotates as it moves along the roadway. As in the case of the bicycle wheel, the tangential velocity at the edge (rim) is approximately twice the drift velocity of the curl's center (wheel hub). Hence the expected drift velocity of the curls is approximately 4 km s^{-1}. The direction of motion of the curls and rays, and their velocities agree well with the predictions from Figure 5.

As expected from the counterclockwise shear (negative slope in panel 3 of Figure 5), arcs A and C form Kelvin-Helmholtz vortex streets. The vortices in arc C, which is close to the magnetic zenith, are observed to be counterclockwise as expected. Arc B also has strong shear in the E x B drifts. However, no vortices were observed in this arc. This situation is quite typical in that vortices are usually observed on the boundaries of a multiple arc, not in its center. Although this has not been modeled, it is presumed that the presence of arcs A and C stabilize arc B against the Kelvin-Helmholtz instability.

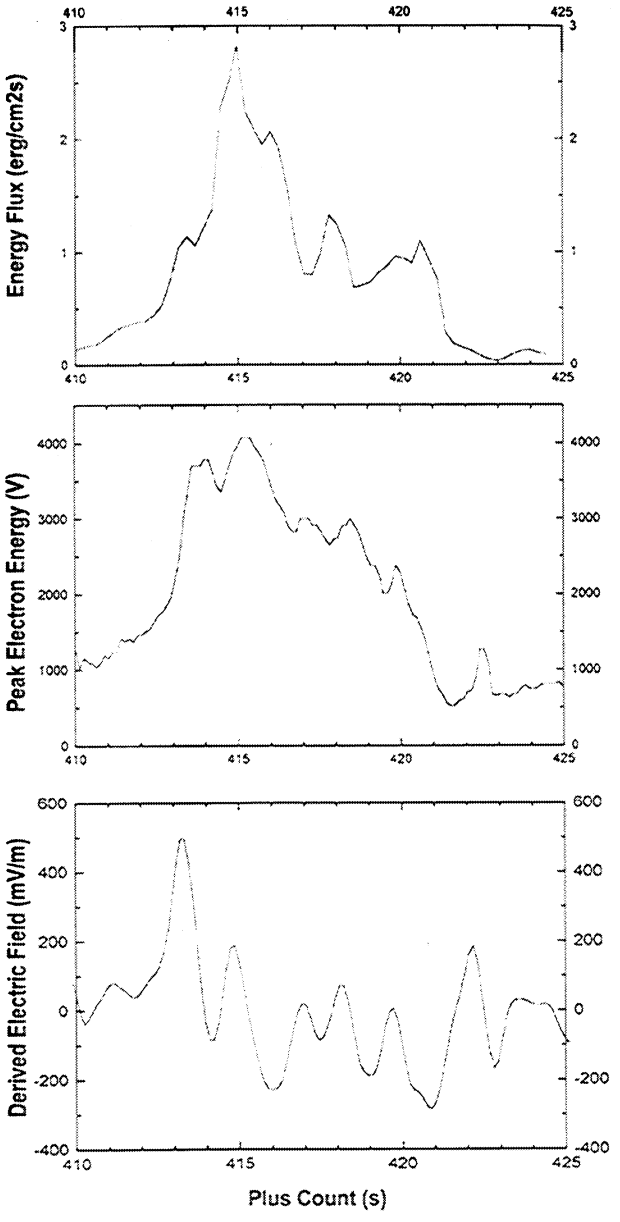

Figure 6. The electron energy flux; peak electron energy, and the inferred perpendicular electric field associated with a vortex street moving along arc C at the same time that the payload traverses the arc.

The fourth panel shows the inferred charge density. The visible arcs correspond to regions of negative charge density. There is excess positive charge both between the arcs and outside the multiple arc structure. The net charge within the multiple arc is slightly negative, giving rise to the non zero potential between the arcs and the counterclockwise drift motions in the auroral rays.

3.3. Vortex Drifts in Arc C

So far we have assumed that the aurora is stable and the payload is traversing a static potential structure. However, if we wish to examine in more detail, it is necessary to consider the auroral motions as well. Particularly for arc C, it is clear that an array of vortices (auroral rays) passed above the payload during

its approximate 5 s passage through the arc. Based on the Kelvin-Helmholtz model, one would expect a concentrated negative potential above each individual ray, and this should be reflected in the electron energy measured at the payload.

The model that we envision is that, above the acceleration region, there is a potential well (negative maximum) associated with each ray or vortex. These potential wells move with the rays. At a point which is fixed or has only a small component of velocity parallel to the ray motion, one would expect a predominantly east-west oscillating electric field. At any given time, the field should point toward the closest ray. In short, if we view this portion of the data with somewhat higher temporal resolution, we should see one or more "inverted Vs" that are associated with individual rays passing through the payload rather than with the passage of the payload through arcs.

With this interpretation it is still possible to infer electric fields from the temporal derivative of the electron energy peak. But the component of the field inferred is along the direction of the ray motion (east-west) rather than being perpendicular to the arc. The appropriate velocity to use is the velocity of the rays relative to the payload (4.8 km s^{-1} eastward) so the westward electric field in mV m^{-1} is

$$E_x = (\delta w/\delta t)/(\delta x/\delta t) = (\delta w/\delta t)/4.8.$$

This field is directed along the direction of the relative velocity which is at an angle of 41 degrees with respect to the rocket trajectory. Thus the field in the direction of the payload antenna is

$$E_{\text{antenna}} = (\delta w/\delta t) \sin (41)/4.8.$$

Figure 6 shows the energy flux, peak energy, and inferred perpendicular (east-west) electric field as the payload passes through the arc and the rays pass through the payload. The inferred electric field has been smoothed with a routine that suppresses frequencies above 1.5 Hz.

The inferred electric field has a peak value of a bit over 400 mV m^{-1} and oscillates with a period of about 1.6 s (f = 0.6 Hz). This is in reasonable agreement with the frequency of rays passing a fixed point (0.68±0.08 Hz) measured in the TV data just to the east of the payload footprint. The amplitude decays as the payload moves polewärd of the arc but is still recognizable well after the energy flux has decayed to a small value.

According to the model, the derived field shown in Figure 3 exists above the acceleration region and is a predominantly east/west field pointed at any given time toward the closest auroral ray. Since the approaching rays come from the west, the initial pulse is westward.

The rocket is well below the acceleration region, and thus the electric field booms cannot sample this field directly. Nonetheless, if there is indeed an oscillating perpendicular electric field just above the acceleration region, it should launch an Alfvén wave along B toward the ionosphere and the payload. The existence of parallel electric fields in the acceleration region may reduce the amplitude of the Alfvén wave, but some remnant is likely to reach the rocket altitude.

Indeed, an Alfvén wave was detected at this time by the payload and had a frequency similar to that of the inferred electric field in Figure 6. To facilitate comparison, the payload electric field data were also smoothed to suppress frequencies above 1.5 Hz as in Figure 6. In Figure 7 we compare the component along the antenna of the inferred electric field with the westward field measured at the payload. For purposes of the comparison we have used separate scales for the measured field and the inferred field and we have delayed the inferred field by 0.8 s to provide the best match. Since the electric fields are

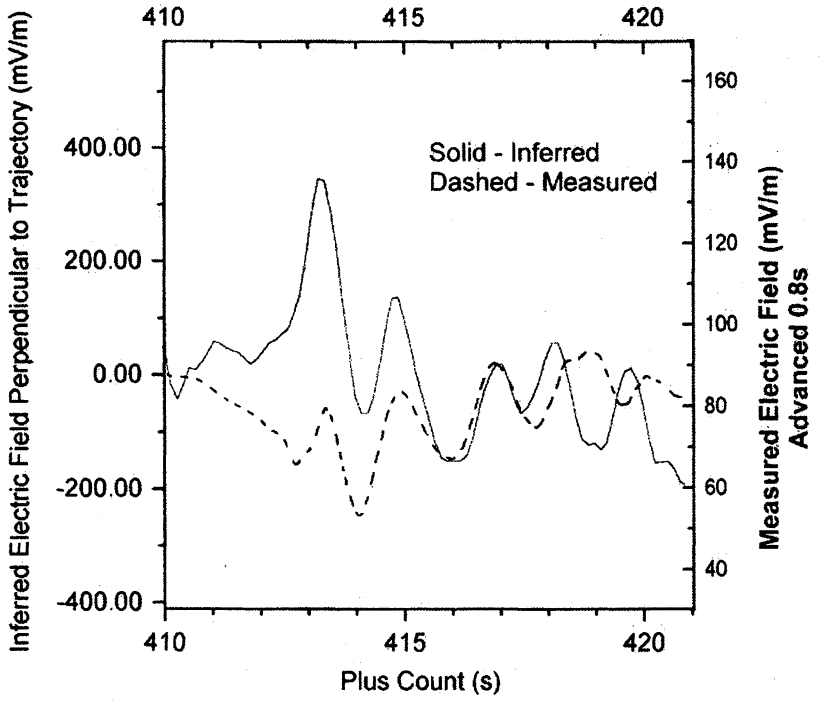

Figure 7. Comparison of the inferred electric field calculated from the peak electron energy with the field measured at the payload. The amplitude scales differ by a factor of eight and the inferred field waveform has been delayed 0.8 s to match the measured field.

quasiperiodic, other delays are allowed. However, 0.8 s is the minimum delay that aligns most of the peaks in the two traces, as well as matching the first positive going pulse in both signals. The measured field appears to have a slightly longer period and is somewhat less damped than the inferred field. It also has an initial negative excursion that does not appear in the inferred field. Nonetheless, at least for the first few cycles, the two waveforms agree reasonably well.

It seems clear that the Alfvén wave is associated with the passage of the auroral rays. Moreover, while the measured field correlates well with the inferred electric field, it does not correlate well with the particle flux, the peak energy, or the energy flux, all of which are dominated by the lower frequency term associated with passage of the payload through the arc.

The 0.8 s delay in the wave data relative to the calculated field is plausibly consistent with the difference in electron and Alfvén wave travel times from the acceleration region to the payload. Energy-dispersed electrons below the energy peak showed dispersions consistent with source altitudes 2000 to 7000 km above the payload. Since the peak energy of the dispersed electrons was well below the inverted V peak energy, the main acceleration region would presumably be somewhere above the source of the energy-dispersed electrons.

Since the wave is only lightly damped and continued to be measured well poleward of the region of significant energy flux, it would seem that the wave spreads poleward. Since this implies a poleward component in its propagation, the poleward motion of the payload could be expected to Doppler shift the wave to a somewhat lower frequency as observed.

3.4. Poleward of the Discrete Arcs

Bonnell [1997] also detected Alfvén waves during the period around 432 s and again at 443 s. Unfortunately, the aiming point of the narrow-field camera was being changed during both of these intervals, so a detailed study similar to the one at 415 s is not practical. These waves appear to be associated with the brief activations of ray motions observed in the poleward arc at these times. Even with the camera moving, it can be shown that the overall envelope of the wave activity coincides with that of the arc brightening. Here again *Bonnell* [1997] concluded that the payload was measuring a composite of Alfvén waves coming from above with reflections from the ionosphere.

4. Summary and Conclusions

The AMICIST flight provided a unique opportunity to study the morphology of overhead rayed arcs and relate them in detail to in situ measurements of particles and waves. The locations and relative intensities of the arcs agreed well with the precipitating energy flux, although the arcs were at a higher altitude than predicted. The high-altitude electric fields predicted from derivatives of the peak electron energy had the correct magnitude and sense to account for the curl formation and for the drift direction and velocity. An oscillating high-altitude electric field predicted to be associated with the moving rays appears consistent with an Alfvén wave measured at the payload. From a detailed comparison of the video images and the in situ data, we conclude the following.

1. In agreement with *Stenbaek-Nielsen et al.* [1998] we find good correlation, down to scale sizes of a few kilometers, between the optical aurora and the precipitated electron energy flux. The actual structure of the aurora is far more readily apparent in linear plots of energy flux than in the more commonly presented electron energy spectra shown on log scales. The altitude of 130 km for the lower border of arc A (determined by matching the all-sky intensity traces to the energy flux plots) implies an energy below 2 keV for the electrons on the equatorward edge of the arc. This is less than the 4-5 keV peak energy for the arc seen in Figure 5. The discrepancy is not understood and more complete modeling of the luminosity distribution is planned. The transient rayed arc at 431s had a lower border altitude of 170 ± 10 km and considerable vertical extent. This agrees at least qualitatively with the energy spectrogram (Plate 1) which shows energies spread from less than 100 eV to about 800 eV. Again, more detailed modeling is planned.

2. The bulk motions of auroral rays in the equatorward and poleward arcs are consistent in magnitude and direction with the high-altitude electric field derived from the spatial gradient of the electron energy peak. This supports the conventional model of electron acceleration by a quasistatic electric field.

3. The shear in the derived electric field within the arcs is appropriate for forming counterclockwise vortex streets as observed in arc C and inferred from the ray motions in arc A. The arcs all have excess negative charge above the acceleration region, consistent with the counterclockwise vortices [*Webster*, 1957].

4. The Alfvén waves detected at the payload have an onset, duration, and frequency that are clearly related to the overhead passage of a Kelvin-Helmholtz vortex street. The frequency of rays passing a point, the frequency of the electric field inferred from the electron energies measured in situ, and the frequency of the Alfvén wave detected at the payload are all 0.6-0.7 Hz. Moreover (except for an 0.8 s delay in the measured Alfvén wave), they all start at the same time. Thus at least one source of Alfvén waves (~0.6 Hz) has been identified. The waves are consistent with the Kelvin-Helmholtz model in which there is an inward directed electric field toward each ray. The overhead passage of the vortex street induces an Alfvén wave phase locked at the source to the rays. The 0.8 s phase shift in the measured wave relative to the inferred high-altitude electric field is interpreted as a propagation time from the source region (strictly speaking, the difference between the Alfvén wave propagation time and the electron transit time). The Alfvén waves at 431 and 443 s [*Bonnell*, 1997] appear to be related to ray motions that are well equatorward of the payload.

Acknowledgments. I thank E. Hoch who developed the program for real-time calculation of the look angles from Kaktovik to the 110 km footprint of the payload. The AMICIST flight was supported by NASA grants NAG5-5007 and NAG5-5057. The optical observations were supported by NASA grant NAG5-5013. The analysis of the optical data has been supported in part by internal Geophysical Institute funds.

Janet G. Luhmann thanks Göran T. Marklund and Bengt Hultqvist for their assistance in evaluating this paper.

Figures 1, 2, and 5 and Plate 1 are reprinted or adapted from Phys. Chem. Earth *26*, T. J. Hallinan and H. C. Stenbaek-Nielsen, The connection between auroral acceleration and auroral morphology, 169-177, Copyright 2001, with permission from Elsevier Science.

References

Banks, P.M., C.R. Chappell, and A.F. Nagy, A new model for the interaction of auroral electrons with the atmosphere: Spectral degradation, backscatter, optical emission, and ionization, *J. Geophys. Res.*, 79, 1459-1470, 1974.

Bonnell, J., P. Kintner, J.-E. Wahlund, K. Lynch, and R. Arnoldy, Interferometric determination of broadband ELF wave phase velocity

within a region of transverse auroral ion acceleration, *Geophys. Res. Lett.,23,* 3297-3300, 1996.

Bonnell, J.W., Identification of broadband ELF waves observed during transverse ion acceleration in the auroral ionosphere, Ph.D. thesis, Cornell Univ., Ithaca, N.Y., 1997.

Carlqvist, P., and R. Bostrom, Space-charge regions above the aurora, *J. Geophys. Res.,* 75, 7140-7145, 1970.

Hallinan, T.J. and T.N. Davis, Small-scale auroral arc distortions, *Planet. Space Sci.,18,* 1735-1744, 1970.

Lynch, K.A., R.L. Arnoldy, P.M. Kintner, and J. Bonnell, The AMICIST auroral sounding rocket: A comparison of transverse ion acceleration mechanisms, *Geophys. Res. Lett.,23,* 3293-3296, 1996.

Mozer, F.S., C.W. Carlson, M.K. Hudson, R.B. Torbert, B. Parady, and J. Yatteau, Observations of paired electrostatic shocks in the polar magnetosphere, *Phys. Rev. Lett., 38,* 292-295, 1977.

Rees, M.H., Auroral ionization and excitation by incident energetic electrons, *Planet. Space Sci., 11,* 1209-1218, 1963.

Stenbaek-Nielsen, H.C., T.J. Hallinan, D.L. Osborne, J. Kimball, C. Chaston, J. McFadden, G. Delory, M. Temerin, and C.W. Carlson, Aircraft observations conjugate to FAST: Auroral arc thicknesses, *Geophys. Res. Lett., 25,* 2073-2076, 1998.

Swift, D.W., H.C. Stenbaek-Nielsen, and T.J. Hallinan, An equipotential model for auroral arcs, *J. Geophys. Res., 81,* 3931-3934, 1976.

Webster, H.F., Structure in magnetically confined electron beams, *J. Appl. Phys., 28,* 1395-1397, 1957.

R. Arnoldy and K. Lynch, Space Science Center, University of New Hampshire, 2 Leavitt Lane, Durham, NH 03824-3518.

J. Bonnell, Space Science Laboratory, University of California, 2000 Center St., Suite 303, Berkeley, CA 94704-1200.

T. J. Hallinan and H. C. Stenbaek-Nielsen, Geophysical Institute, University of Alaska Fairbanks, 903 Koyukuk Drive, P.O. Box 757320, Fairbanks, AK 99775-7320. (hallinan@dino.gi.alaska.edu).

J. Kimball, Johnson Space Center, 2101 NASA Rd. 1, Houston, TX 77058-3691.

P. Kinther, School of Electrical Engineering, Cornell University, Ithaca, NY 14853-0001.

(Received August 21, 2000; revised October 19, 2000;
accepted October 19, 2000.)